

# The role of oxidizing conditions in the dispersion of supported platinum nanoparticles evaluated via ab initio atomistic modeling

Agustin Salcedo, David Loffreda, and Carine Michel\*

*ENS de Lyon, CNRS, Laboratoire de Chimie UMR 5182, 46 allée d'Italie, F-69364 Lyon  
France*

E-mail: carine.michel@ens-lyon.fr

## Abstract

Achieving fine control over platinum (Pt) dispersion is a promising avenue to tailor catalysts for specific applications and enhance their activity and selectivity. Experimental observations suggest that exposing ceria-supported Pt particles to O<sub>2</sub> at 500 °C promote their dispersion into smaller particles and eventually single-atoms. ~~Still,~~ the exact role of oxygen in the redispersion is not well-understood yet. Past density-functional theory studies of ceria-supported Pt have narrowed down their scope to specific particle sizes, typically single atoms and small clusters. Herein we combine several approaches and types of models in a consistent atomistic framework to evaluate the relative stability of ceria-supported Pt as a function of the degree of oxidation of Pt and of the particle size, ranging from single atoms to nanoparticles of 1.5 nm of diameter. We find that the largest nanoparticles remain the **most stable species** on **the lowest energy facet of ceria** even under oxidizing conditions, suggesting that stronger adsorption sites are required to stabilize smaller particles and single-atoms and promote oxidative dispersion.

# Introduction

The electronic structure, surface properties, stability, and poisoning resistance of platinum make it an exceptional catalyst for a variety of industrial processes, including selective hydrogenation and dehydrogenation reactions,<sup>1,2</sup> water-gas shift (WGS) for H<sub>2</sub> production,<sup>3,4</sup> non-oxidative coupling of methane,<sup>5,6</sup> dealkylation of toluene,<sup>7,8</sup> isomerization of hydrocarbons,<sup>9,10</sup> oxidation of CO and NO,<sup>11</sup> and the electrocatalytic hydrogen evolution and oxygen reduction reactions,<sup>12</sup> among others.

Depending on the application, different Pt particle sizes may be preferred. Achieving fine control over the particle size (dispersion) and tailoring the catalyst for its specific application is a promising approach for enhancing the activity and selectivity. However, like other noble metal catalysts, Pt suffers from sintering, i.e. the process of agglomeration or coalescence of single atoms and small particles into larger ones, which results in a decrease in the surface area, leading to a reduction in the number of available active sites and the catalytic activity (degradation).<sup>13-15</sup> Sintering typically takes place at reaction temperatures above 500 °C, although this is dependant on the support and gas mixture composition.<sup>16,17</sup> Careful engineering of the catalytic particles and their interactions with the support can mitigate the sintering process. Some strategies in that regard include optimization of the Pt concentration and uniformity,<sup>15</sup> encapsulation in a metal oxide shell or other protective layers,<sup>18</sup> incorporation in porous supports like zeolites,<sup>19</sup> and doping of the support.<sup>20</sup> Nevertheless, such strategies only slow down the sintering, and cannot prevent it from occurring under operating conditions.

For this reason, there is an increasing interest in developing protocols that make use of the structural dynamics of the catalyst to control Pt dispersion and tune the particle size in situ at mild operating conditions, by cycling between oxidative and reductive conditions.<sup>21</sup> To tune the Pt dispersion via redox cycling, cerium oxide (ceria) has been proposed as a viable support since its stronger interaction with Pt compared to the classic Al<sub>2</sub>O<sub>3</sub> support allows a more gradual evolution of the particle size and morphology.<sup>22,23</sup> In particular, it

has been recently shown that oxidative treatments exposing the catalyst to 1.5 mbar of O<sub>2</sub> at ~500 °C promote the dispersion of Pt nanoparticles into smaller oxidized Pt species, eventually forming Pt single atoms, which can be exploited in a controlled manner to enhance the catalyst’s performance for low-temperature CO oxidation.<sup>24–26</sup>

The current understanding of the oxidative dispersion phenomenon remains very limited.<sup>27</sup> Strong metal-support interactions lower the barrier for the spillover of Pt atoms from parent nanoparticles, to form new bonds with the support. However, this is usually conducive to sintering rather than dispersion, by a process known as Ostwald ripening, involving the migration of dissociated atoms and their incorporation into larger nanoparticles.<sup>28–30</sup> Nevertheless, spillover might also lead to atomically dispersed Pt species, provided they are effectively trapped by the support.<sup>30,31</sup> The larger spacing between nanoparticles at low coverage increases the probability of atoms being captured by strong adsorption sites rather than colliding with nanoparticles.

Overall, many questions remain regarding the factors governing the dispersion process, such as the role of oxygen, explaining the need for oxidative conditions, and the types of sites required for trapping Pt single atoms. The experimental investigation of these questions is challenging, since characterization techniques such as TEM display weak contrast for atomically dispersed species and small oxidized clusters, and thus cannot conclusively differentiate them.<sup>31,32</sup> For this reason, theoretical studies constitute a promising avenue to shed light on this phenomenon and understand the transition from Pt nanoparticles to single atoms.

~~In this sense,~~ past theoretical studies of ceria-supported Pt have focused on single-atom models, because of their relevance as single-atom catalysts (SACs) for a variety of reactions.<sup>32–36</sup> Extensive literature reporting DFT studies of the structure and stability of atomically dispersed Pt on both low-index and high-index (stepped) surfaces is available.<sup>25,27,37–40</sup> The gas-phase structure and adsorption configuration of Pt<sub>1</sub>O<sub>y</sub> species and their interaction with the ceria support is well documented in these works, and has been taken as a reference

in this work. On the other hand, computational studies of Pt nanoparticles are rare in the literature, and usually disregard the support and focus on understanding finite-size effects and establishing d-band correlations for isolated nanoparticles.<sup>41–45</sup> Recent works have begun to consider the dynamic structure of supported Pt nanoparticles exposed to reactants, by combining ad-hoc cluster models,<sup>46–49</sup> global optimization,<sup>50</sup> and large nanoparticles derived from the bulk or gas-phase structures.<sup>51–53</sup>

In this work, we aim to gain atomic-level insight into the oxidative dispersion of Pt nanoparticles supported ceria, by performing a computational density functional theory (DFT) study combining all of the previously discussed approaches in a consistent theoretical framework to evaluate the relative stability of  $\text{Pt}_x\text{O}_y$  species as a function of size and degree of oxidation and identify the thermodynamically favorable oxidizing conditions for Pt dispersion. Heuristic exploration of adsorption sites and stochastic sampling via grand canonical genetic algorithms and ab-initio molecular dynamics are combined with literature input, to generate models of ceria-supported Pt single atoms, subnanometer rafts, and nanoparticles of diameter larger than 1 nm, both reduced and oxidized.

## Methods

### Computational details

Density functional theory (DFT) calculations were performed using VASP 6.2.1.<sup>54,55</sup> The exchange-correlation energy was calculated within the generalized gradient approximation (GGA), with the Perdew-Burke-Ernzerhof (PBE) exchange-correlation functional.<sup>56</sup> Long-range dispersion was implemented using Grimme’s D3(BJ) correction.<sup>57,58</sup> The valence electrons were treated on a plane-wave basis with an energy cutoff of 400 eV, whereas the core electrons were represented with the projector-augmented wave (PAW) method.<sup>59</sup> Total energies were calculated with a numeric precision of  $10^{-6}$  eV ( $10^{-5}$  for the genetic algorithm sampling). The DFT+U approach was implemented with Dudarev’s scheme,<sup>60</sup> to consider

strong electronic correlation effects due to charge localization and compensate for the self-interaction error,<sup>61–65</sup> with  $U_{\text{eff}}$  set to 4.5 eV for Ce(4f).<sup>66,67</sup> The forces were converged to  $\pm 0.02$  eV/Å. The Brillouin zone was sampled using a  $2 \times 2 \times 1$  k-point grid for  $(3 \times 3)$  cells, and only the gamma point for larger cells, namely  $(4 \times 4)$ ,  $(6 \times 6)$  and  $(8 \times 8)$ .

## Models

To study the oxidation and redispersion of ceria-supported Pt, the CeO<sub>2</sub>(111) surface was selected, since it is the most stable low-index surface of ceria, and thus the most abundant in polycrystalline catalysts. The surface was modeled using supercells derived from the CeO<sub>2</sub> bulk with the equilibrium lattice parameter of  $a_0 = 5.455$  Å, and consisting of 6 atomic layers (two O–Ce–O trilayers, TL) separated by a 23 Å vacuum layer. A  $(3 \times 3)$  expansion was used for Pt<sub>1</sub>O<sub>x</sub> systems,  $(3 \times 3)$ – $(4 \times 4)$  for Pt<sub>2</sub>O<sub>x</sub>, and  $(4 \times 4)$ – $(6 \times 6)$  for Pt<sub>13</sub>O<sub>x</sub>, and  $(6 \times 6)$ – $(8 \times 8)$  for Pt<sub>147</sub>O<sub>x</sub> systems, to ensure a sufficiently long distance between periodic replicas of the adsorbed Pt nanoparticles, to prevent undesired interactions between them. To account for the Ce<sup>4+</sup>/Ce<sup>3+</sup> redox couple, spin-polarization was allowed in all calculations, except for those of 147-atom nanoparticles, due to the computational cost.

Pt single-atom structures were generated in accordance with the extensive literature on these types of systems, where the most stable structures have been reported after exploration of the adsorption sites of the surface.<sup>25,37–40</sup> Single Pt atoms adsorb twofold bridge position on the CeO<sub>2</sub>(111) surface and adopt a triplet spin multiplicity (Figure 1a) ( $d_{\text{Pt–O}} = 2.00$  Å).<sup>37</sup> The adsorption on oxygen vacancies is stronger,<sup>38,68</sup> but the presence of such vacancies is not expected under oxidizing conditions.<sup>69</sup> Regarding oxidized Pt single atoms, PtO binds linearly on top of surface oxygen (O<sub>surf</sub>), forming a O–Pt–O<sub>surf</sub> species (Figure S1c). PtO<sub>2</sub> adsorbs forming a Pt–O<sub>surf</sub> (2.31 Å) and a O–Ce bond (1.97 Å), with the remaining O atom pointing away from the surface (Figure 2a). An alternative configuration forming two O–Ce bonds is less stable by 0.23 eV (Figure S1d). Finally PtO<sub>3</sub> adopts a twofold configuration with two O–Ce bonds (2.48 Å) and the third O atom pointing up (Figure S1f). Details are

provided in Tables S1 and S2.

Figure 1: Top and side views of the structure of non-oxidized Pt atom and Pt nanoclusters supported on  $\text{CeO}_2(111)$ . (a) Pt single atom,  $(3 \times 3)$  cell. (b)  $\text{Pt}_2$  dimer,  $(3 \times 3)$  cell. (c)  $\text{Pt}_{13}$  cluster,  $(4 \times 4)$  cell. (d)  $\text{Pt}_{147}$  nanoparticle,  $(6 \times 6)$  cell. Ce in gray, surface O in light red, subsurface O in dark red, Pt in blue.

Figure 2: Top and side views of the structure of oxidized  $\text{Pt}_x\text{O}_{2x}$  species supported on  $\text{CeO}_2(111)$ . (a)  $\text{PtO}_2$ ,  $(3 \times 3)$  cell. (b)  $\text{Pt}_2\text{O}_4$ ,  $(4 \times 4)$  cell. (c)  $\text{Pt}_{13}\text{O}_{26}$  cluster,  $(6 \times 6)$  cell. (d)  $\text{Pt}_{147}\text{O}_{294}$  nanoparticle,  $(8 \times 8)$  cell. Ce in gray, surface O in light red, subsurface O in dark red, excess O (with respect to the support’s stoichiometry and defined as belonging to the Pt oxide) in orange, Pt in blue.

The  $\text{Pt}_2$  structure is based in the literature as well. For oxidized  $\text{Pt}_2\text{O}_y$  systems, a grand canonical genetic algorithm (GCGA) was used to generate 100  $\text{Pt}_2\text{O}_y/\text{CeO}_2(111)$  structures, and the most competitive ones were selected for each stoichiometry, i.e. for each O/Pt ratio (Figure S2). The genetic algorithm was implemented using the GOCIA package.<sup>70</sup> In this process, the number of Pt atoms is fixed to 2, and the system is allowed to exchange oxygen with a reservoir with a given  $\text{O}_2$  chemical potential. The chemical potential is derived from statistical thermodynamics, setting the temperature to 500 °C and the partial pressure of  $\text{O}_2$  to 0.2 bar. The resulting  $\text{Pt}_2$  dimer binds asymmetrically, with  $\text{Pt}-\text{O}_{\text{surf}}$  bonds of 1.91 Å and 1.98 Å (Figure 1b). On the other hand,  $\text{Pt}_2\text{O}_4$  adsorbs in a symmetric configuration forming two  $\text{Pt}-\text{O}_{\text{surf}}$  bonds (2.03 Å) and two O–Ce bonds (Figure 2b). Table S3 summarizes all the structures generated by the genetic algorithm.

For  $\text{Pt}_{13}\text{O}_y$  clusters, three different competitive 13-atom starting geometries were considered, namely cuboctahedron ( $\text{Pt}_{13}\text{cubo}$ ), Mackay icosahedron ( $\text{Pt}_{13}\text{ico}$ ), and ino truncated decahedron ( $\text{Pt}_{13}\text{ino}$ ) (Figure S3a–c). The latter is the most stable in vacuum, with  $\text{Pt}_{13}\text{cubo}$  being less stable by 0.34 eV and  $\text{Pt}_{13}\text{ico}$  by 0.46 eV. These clusters were adsorbed on the  $\text{CeO}_2(111)$  surface and covered with oxygen at two different oxygen contents:  $\text{Pt}_{13}\text{O}_7$  and  $\text{Pt}_{13}\text{O}_{13}$ . Due to the large fluxionality at this cluster size, geometry optimization may result in structures very far from the global minimum, whereas sampling via genetic algorithms be-

comes too expensive at this supercell slab size. For this reason, a search for more competitive structures was done via annealing of each of the three starting geometries, by performing ab initio molecular dynamics (AIMD) calculations with a time step of 5 fs and a velocity rescaling thermostat at 800 K to sample a variety of configurations for  $\sim 10$  ps. The lowest potential energy frame of each trajectory was selected and quenched back to 0 K by geometry optimization (Table S4). The most stable structure for each stoichiometry was selected as the representative model. For the clean Pt<sub>13</sub> cluster the AIMD simulation lead to a bilayer 8+5 cluster, as shown in Figure 1c, whereas oxide clusters adopt amorphous structures (Figure S4). A fourth stoichiometry Pt<sub>13</sub>O<sub>26</sub> was obtained by extracting a 2-layer fragment from the bulk of hexagonal  $\alpha$ -PtO<sub>2</sub>, adsorbing it on CeO<sub>2</sub>(111) and carrying out the same annealing procedure (Figure 2c).

Finally, to model the Pt nanoparticles of a size larger than 1 nm, the most stable high-symmetry isomer of Pt<sub>147</sub> in gas-phase was selected, namely a strongly irregular truncated octahedron, with a diameter of  $\sim 1.5$  nm (Figure S3d).<sup>71</sup> This nanoparticle exhibits a variety of (100)- and (111)-type facets offering diverse adsorption sites for oxygen atoms. Adsorption of oxygen on the nanoparticle was first examined by probing several adsorption sites for single atoms and 3-atom arrangements (see Table S5). From this we obtained general guidelines for the “decoration” of the nanoparticle with oxygen atoms, such as: (i) adsorption on the edges is favorable over adsorption on the facets, (ii) edges between a (100) and a (111) facet are preferred, where O adsorbs twofold, followed by edges between two (111) facets, where O adsorbs on fcc sites near the edges and distributing between the two facets, (iii) on (111) facets, fcc sites are preferred, (iv) adsorption on subsurface sites is not favorable at low coverage. With this information, models with 33, 47, and 80 oxygen atoms were proposed (corresponding to coverages of 0.33–0.83, with coverage defined as the ratio between adsorbed O and surface Pt). Subsequently, AIMD calculations were run using a velocity rescaling thermostat at 800 K with a time step of 5 fs, to find better local minima by sampling variations on the adsorption sites due to coverage effects accessible within reasonably short

MD trajectories (< 3 ps). The lowest potential energy points were selected and optimized.

The clean Pt<sub>147</sub> and the O-covered Pt<sub>147</sub>O<sub>y</sub> nanoparticles were adsorbed on CeO<sub>2</sub>(111) (Figures 1d and S5a–d), with their largest facet in contact with the support, to maximize the Pt-ceria interaction, forming 14 Pt–O<sub>surf</sub> bonds. Oxygen was removed from the adsorption facet, so the resulting systems are Pt<sub>147</sub>O<sub>32</sub>, Pt<sub>147</sub>O<sub>43</sub> and Pt<sub>147</sub>O<sub>72</sub> adsorbed on CeO<sub>2</sub>(111).

Attempts to obtain nanoparticles with a higher coverage by following the aforementioned protocol (adsorption of O atoms) resulted in the formation of O<sub>2</sub> molecules, indicating that 0.83 approaches the surface saturation coverage for this nanoparticle. Therefore, to consider a higher O/Pt ratio, platinum oxide nanoparticles were generated. Pt<sub>147</sub>O<sub>147</sub> was modeled as a core-shell cluster, by removing the exposed outer shell of the Pt<sub>147</sub> nanoparticle supported on CeO<sub>2</sub>(111), and replacing it with an equivalent shell (same number of Pt atoms) derived from the bulk of hexagonal  $\alpha$ -PtO<sub>2</sub> (Figure S5e). On the other hand, Pt<sub>147</sub>O<sub>294</sub> was generated directly from the bulk, extracting a 3-layer fragment and adsorbing it on CeO<sub>2</sub>(111) as is (Figure 2d and S5f). Details are provided in Table S6.

## Results and Discussion

To understand the effect of the oxidizing environment on the dispersion of Pt species supported on cerium oxide, we evaluate the Gibbs free energy of formation per Pt atom ( $\Delta G_f$ ) for all the different sizes considered, namely single atoms, dimers, Pt<sub>13</sub> clusters, and Pt<sub>147</sub> nanoparticles, using ab initio atomistic thermodynamics and assuming equilibrium with a gas reservoir of fixed temperature and pressure.  $\Delta G_f(T, P_{O_2})$  is calculated as follows:

$$x \text{ Pt} + \text{CeO}_2 + \frac{y}{2} \text{O}_2(\text{g}) \longrightarrow \text{Pt}_x\text{O}_y/\text{CeO}_2$$

$$\Delta G_f(T, P_{O_2}) = \frac{1}{x} (E_{\text{Pt}_x\text{O}_y/\text{CeO}_2} - TS_{\text{conf}} - xE_{\text{Pt}} - E_{\text{CeO}_2} - \frac{y}{2}\mu_{\text{O}_2}(T, P_{O_2}))$$

Where  $E_{\text{Pt}_x\text{O}_y/\text{CeO}_2}$  is the total electronic energy of the supported Pt species provided by the DFT calculations,  $E_{\text{Pt}}$  and  $E_{\text{CeO}_2}$  are those of the **isolated Pt single atom** and the CeO<sub>2</sub>(111)



surface, and  $\mu_{\text{O}_2}$  is the chemical potential of  $\text{O}_2$ , which is a function of temperature and partial pressure of  $\text{O}_2$ . Details on the calculation of this chemical potential can be found in the Supporting Information. Finally,  $S_{\text{conf}}$  is the configurational entropy, calculated as follows:<sup>72</sup>

$$S_{\text{conf}} = k_B \frac{n_{\text{sites}}!}{(n_{\text{sites}} - n_{\text{species}})!n_{\text{species}}!}$$

In this equation, for a given  $\text{Pt}_x\text{O}_y/\text{CeO}_2$  system,  $n_{\text{species}} = 147/x$  is the number of Pt species to distribute on the ceria surface, and  $n_{\text{sites}} = n_{\text{species}}/0.1$  the number of free sites those species can occupy. 0.1 is a coverage factor, to compare all systems at equivalent content of Pt. Under this approach, we account for the difference in the nature of the adsorption site at different particle sizes, simply by assuming that an adsorption site for a  $\text{Pt}_x\text{O}_y$  nanoparticle corresponds to  $x$  adsorption sites for a  $\text{Pt}_1\text{O}_y$  species. The configurational entropy reflects the number of ways in which the Pt species can be spatially arranged on the ceria surface. Although this contribution is typically disregarded in the calculation of adsorption free energies of reactants and products, when considering a single adsorbed Pt species that splits into hundreds of individual species, the change in configurational entropy is significant, and thus it must be considered in the study of the dispersion process.

In the following subsections we use the free energy of formation as a stability descriptor, focusing first on investigating the gradual oxidation of Pt species adsorbed on  $\text{CeO}_2(111)$  at different sizes separately, and next comparing them with each other, at simulated conditions equivalent to the experimental ones, to evaluate the dispersion of large nanoparticles into smaller particles or single atoms.

## Oxidation of platinum

$\Delta G_f$  can be calculated for a grid of temperatures and pressures to generate phase diagrams showing the thermodynamically stable content of oxygen at different conditions for each particle size (Figure 3).

Figure 3: Thermodynamic phase diagrams of Pt/CeO<sub>2</sub>(111) under oxidizing conditions. The evaluated temperature and pressure ranges are 450–1550 K and 1.10<sup>-4</sup>–5.10<sup>-2</sup> bar, respectively. (a) Pt<sub>147</sub> nanoparticles, (b) Pt<sub>13</sub> clusters, (c) Pt<sub>2</sub> dimers and (d) Pt single atoms.

We observe that Pt<sub>x</sub>O<sub>2x</sub>-type oxide species remain the most stable structures even at low O<sub>2</sub> pressure up to ~900 K. Only at very high temperature the desorption of O<sub>2</sub> to the gas phase becomes favorable stabilizing structures with lower oxygen content.

In the case of the Pt<sub>147</sub> nanoparticle, all the spectrum from metallic Pt<sub>147</sub> to Pt<sub>147</sub>O<sub>294</sub> is observed within the temperature range evaluated, although very high temperatures are required to stabilize non-oxidized Pt<sub>147</sub> particles. In addition, Pt<sub>147</sub>O<sub>147</sub> does not appear in the diagram, indicating it is not the most stable state at any combination of temperature and pressure. This result could reflect that such an stoichiometry occurs only as a short-lived intermediate state in the transition from O-covered Pt to Pt oxide, but it could also be ascribed to the fact that the Pt<sub>147</sub>O<sub>147</sub> species that we have evaluated is far from the global minimum. Either way, we can conclude that at the Pt dispersion temperature (500 °C = 773.15 K), a highly oxidized nanoparticle is the most stable species.

In the case of smaller systems, the non-oxidized species do not appear in the diagram, and O/Pt ratios lower than 2 become harder to access. For instance, Pt<sub>13</sub>O<sub>7</sub>, corresponding to an O/Pt ratio of about 0.5, is stable at high temperatures for Pt<sub>13</sub>, but the equivalent Pt<sub>2</sub>O<sub>1</sub> species is not stable in this temperature range. Similarly, for a pressure of 1.5 mbar, the transition from Pt<sub>13</sub>O<sub>26</sub> to Pt<sub>13</sub>O<sub>13</sub> takes place at 860 K, whereas for the equivalent transition from Pt<sub>2</sub>O<sub>4</sub> to Pt<sub>2</sub>O<sub>2</sub> a temperature of 1102 K is required. Overall, these thermodynamic phase diagrams suggest that small Pt species can only be present in oxidized form, regardless of temperature. This is consistent with experiments in the literature showing that reductive treatments result in an increase in particle size (sintering), rather than in the formation of reduced single atoms.<sup>26,69</sup>

To understand why it is easier to oxidize Pt as the nanoparticle size decreases we calculate

the 0 K oxidation energy, i.e. the energy released in the reaction  $\text{Pt}_x + x \text{O}_2(\text{g}) \longrightarrow \text{Pt}_x\text{O}_{2x}$  (Figure 4). We find that this phenomenon can be associated almost exclusively with changes in the intrinsic stability of the Pt species, and is rather independent of the interaction with the ceria support. This can be inferred first from the comparison of the oxidation energy of an isolated Pt species to  $\text{PtO}_2$ , of  $\Delta E_{\text{ox}} = -5.63$  eV, with the corresponding oxidation energy of bulk Pt to bulk  $\alpha\text{-PtO}_2$ , which is only  $\Delta E_{\text{ox}} = -2.83$  eV per Pt atom. Although the stoichiometry is the same in both cases, significantly less energy is gained when oxidizing bulk Pt than when oxidizing isolated Pt atoms. This is most likely because of the varying coordination of Pt. An isolated Pt atom gains 2 Pt–O bonds ( $d_{\text{Pt-O}} = 1.70$  Å) when oxidized to  $\text{PtO}_2$ , and loses no bond. Instead, in bulk fcc Pt ( $d_{\text{Pt-Pt}} = 2.78$  Å) each atom has a coordination number of 12, giving a formation energy from isolated Pt of  $-6.25$  eV, whereas in oxidized bulk  $\text{PtO}_2$ , each Pt atom has 6 oxygen atoms in its first sphere of coordination ( $d_{\text{Pt-O}} = 2.03$  Å), and 5 Pt atoms further away second sphere ( $d_{\text{Pt-Pt}} = 3.17$  Å), and the formation energy from isolated  $\text{PtO}_2$  species is only  $-3.45$  eV, thus making the oxidation of bulk Pt less exothermic.

Figure 4: Energy involved in the oxidation of  $\text{Pt}_x$  species to the corresponding  $\text{Pt}_x\text{O}_{2x}$  species at 0 K.

Following the same trend, the oxidation of species in between  $\text{PtO}_2$  molecules and bulk  $\text{PtO}_2$  should fall in between, i.e. more favorable than the bulk but less than a single atom, and indeed we observe this behavior for the oxidation of isolated  $\text{Pt}_2$  and  $\text{Pt}_{13}$  species to  $\text{Pt}_2\text{O}_4$  and  $\text{Pt}_{13}\text{O}_{26}$ . In the case of  $\text{Pt}_{147}$ , the oxidation seems to be even less exothermic than that of the bulk, but we ascribe this result to the limitations in the generation of the model, since global optimization is not computationally viable at this size. In other words, there should exist a more stable oxidized  ~~$\text{Pt}_{147}\text{O}_{294}$~~  nanoparticle than the one proposed in this work, in which case the oxidation of  $\text{Pt}_{147}$  would be more exothermic than the oxidation of the Pt bulk.

Regarding the effect of the support, we observe that its impact on the 0 K oxidation energy

is more significant for single atoms (change of 1.22 eV) than for larger clusters (changes under 0.31 eV) (cf. red bars in Figure 4), and overall it does not change the trend previously described.

Having identified the trends for each Pt particle size, in the following section we address the question of the competition between these different particle sizes under oxidizing conditions, to gain insight into the processes of dispersion of Pt supported on ceria.

## Dispersion of platinum

The stabilization of species of different sizes depends on a variety of factors, including the Pt–ceria interaction, the formation of Pt–Pt bonds, and the configurational entropy at a given coverage. These properties rule whether or not Pt nanoparticles can be redispersed into single atoms reversing the sintering process.

To study the dispersion of this nanoparticle under oxidizing conditions, the collection of structures considered before are compared at fixed oxidative conditions of temperature and pressure, namely 500 °C and ambient pressure of O<sub>2</sub> (0.21 bar), as shown in Figure 5a.

Figure 5: (a) Free energy of formation of the Pt/CeO<sub>2</sub>(111) systems under oxidizing conditions ( $T = 773.15$  K,  $P_{\text{O}_2} = 0.21$  bar). The dash line correspond to the free energy of formation of clean Pt<sub>147</sub>. Note that Pt<sub>13</sub>O<sub>26</sub> and Pt<sub>147</sub>O<sub>294</sub> are very close in energy (a difference of 0.02 eV/Pt atom), so they appear overlapped. (b) Number of Pt–Pt bonds per Pt atom. (c) Number of Pt–O bonds per Pt atom.

The results indicate that single atoms are not accessible under these conditions, since the difference in  $\Delta G_f$  between any of the systems considered and Pt<sub>147</sub>/CeO<sub>2</sub> is greater than zero (i.e. the points are above the dash line in Figure 5a), except for the case of PtO<sub>3</sub>, for which it is slightly exergonic. The contribution of the configurational entropy, despite being relatively small, plays a role in this comparison, since its impact on the free energy of formation of single-atom systems (about 0.1 eV) is higher than on that of large nanoparticles. In fact, the inclusion of this contribution changes whether the dispersion of Pt<sub>147</sub> into PtO<sub>3</sub> is predicted to be exergonic or not. Nevertheless, even when considering the configurational

entropy, the formation of  $\text{PtO}_3$  is still less favorable than a simple oxidation of  $\text{Pt}_{147}$  into  $\text{Pt}_{147}\text{O}_{294}$ , which involves no Pt dispersion.

Therefore, these calculations suggests that the oxidizing treatment at 500 °C cannot disperse Pt particles into single atoms on the  $\text{CeO}_2(111)$  surface. This is in line with previous studies showing that single Pt atoms are stabilized the most on  $\text{CeO}_2(111)$  by oxygen vacancies,<sup>68</sup> which would be mostly unavailable under oxidizing conditions. Although the oxidative dispersion of Pt nanoparticles into single atoms has been observed experimentally at very high temperatures of 800 °C,<sup>27</sup> under those conditions the dispersion has been explained as the product of a reconstruction of the ceria support, which takes place due to the very high temperature and the interaction of ceria with Pt, and results in the formation of step edges and (100)-type sites where Pt single atoms adsorb more strongly.<sup>40,47</sup> Such a surface reconstruction is not expected at 500 °C.

Furthermore, although the oxidation has a more significant stabilizing effect on smaller Pt species compared to large nanoparticles, which reduces the gap in stability between them, overall the dispersion of the large nanoparticle into smaller clusters remains unfavorable with respect to a simple oxidation of the large nanoparticle with no dispersion. In the case of  $\text{Pt}_{13}$ , upon oxidation to  $\text{Pt}_{13}\text{O}_{26}$  its stability becomes comparable to that of  $\text{Pt}_{147}\text{O}_{294}$ , suggesting its formation could be competitive depending on kinetics, but in absolute terms  $\text{Pt}_{147}\text{O}_{294}$  is still lower in energy (see Tables S4 and S6). Overall, for any given O/Pt ratio, the largest nanoparticle is always the most favorable structure among the ones evaluated.

This can be understood by looking at the evolution in the number of Pt–Pt and Pt–O bonds as a function of the O/Pt ratio, for each particle size considered (Figures 5b and c), normalized by the number of Pt atoms in the particle. In this analysis the label Pt–O comprises both the bonds to oxygen belonging to the ceria surface and additional oxygen incorporated upon oxidation. We observe that single atoms and dimers incorporate oxygen without cleavage of any Pt–Pt bond. However, a small number of Pt atoms also means the number of Pt–O bonds formed is limited, going from 2 in Pt to 4 in  $\text{PtO}_3$ , and from 1 in  $\text{Pt}_2$

to 4 in  $\text{Pt}_2\text{O}_4$ . On the other hand, larger particles lose Pt–Pt bonds upon oxidation, which has a destabilizing effect, but this is compensated by a faster formation of Pt–O bonds (on average, 3 Pt–O bonds are formed per O atom added to the  $\text{Pt}_{147}$  nanoparticle), resulting in an increase from 0.1 in  $\text{Pt}_{147}$  to 5.3 in  $\text{Pt}_{147}\text{O}_{294}$ . Moreover, the Pt–O bond is stronger than the Pt–Pt bond (0.52 against 2.36 eV, in the respective Pt and  $\text{PtO}_2$  bulks), and thus it has a stronger stabilizing effect. Thus, the formation of Pt–O bonds compensates the loss of Pt–Pt bonds making the larger nanoparticles the most stable systems regardless of the degree of oxidation. The complete bond analysis is presented in Table S7.

In summary, the results presented here indicate that although dispersed  $\text{PtO}_y$  species are stabilized respect to single Pt atoms under oxidizing conditions, larger nanoparticles remain the most stable Pt species on the  $\text{CeO}_2(111)$  surface. In other words, oxidation is not sufficient to achieve the redispersion observed experimentally, suggesting that the trapping of single atoms must be promoted by a different factor, possibly their interaction with contaminants ( $\text{OH}^-$ ,  $\text{Cl}^-$ ), which could strengthen the binding to the support,<sup>73–75</sup> or the adsorption on surface defects such as step edges which favor smaller particles.<sup>27,76,77</sup> In this sense, nanostructuring the support to maximize the availability of these types of sites could be necessary to achieve a quantitatively significant dispersion of Pt and establish sintering-redispersion cycles for the regeneration of ceria-supported Pt catalysts.

## Conclusions

We present a computational DFT study of the dispersion of Pt, evaluating various particle sizes ranging from clusters of about 1.5 nm of diameter to single atoms, and comparing them under the same theoretical framework. To generate representative models, we employ diverse methods, selected depending on the target size and corresponding complexity and computational cost. In particular, we model four different particle sizes:  $\text{Pt}_1$ ,  $\text{Pt}_2$ ,  $\text{Pt}_{13}$ , and  $\text{Pt}_{147}$ , at varying degrees of oxidation. Single-atom models are obtained by comprehensive

exploration of the surface adsorption sites, from the literature.  $\text{Pt}_2$  and  $\text{Pt}_{13}$  require more sophisticated sampling methods like genetic algorithms and ab initio molecular dynamics. Finally, large supported  $\text{Pt}_{147}$  nanoparticles are derived from chemical intuition and DFT calculations in vacuum, since sampling is not viable at this size due to the high computational cost.

We find that Pt oxide species are prevalent and difficult to reduce at subnanometer particle sizes, for a wide range of temperatures and pressures. Metallic Pt species only become thermodynamically favorable for the case of larger particle sizes at high temperatures. With respect to the dispersion of Pt,  $\text{Pt}_{147}$  particles remain more stable than smaller particles, regardless of the oxygen content, indicating that the dispersion of Pt is not favorable on this surface. To stabilize Pt single atoms a stronger metal-support interaction is required, suggesting that the dispersion observed experimentally must occur at specific sites of ceria where the adsorption of Pt single atoms is more favorable.

In conclusion, this work provides insight into the relative stability of Pt on the most stable  $\text{CeO}_2(111)$  surface across a wide range of particle sizes and degrees of oxidation. Our findings suggest that stronger adsorption sites are required for Pt dispersion into single atoms. Potential sites satisfying these conditions include those of doped-ceria, as well as sites on other low-index and high-index facets in nanostructured ceria, which will be studied in future works.

## Acknowledgement

The authors acknowledge financial support from Agence National de la Recherche (ANR-19-CE05-0038 PRCI DYCAT project) and the Deutsche Forschungsgemeinschaft (DFG 431423888 DYCAT project). The authors thank the DYCAT partners at IRCElyon and KIT for fruitful discussions. Access to national HPC resources of IDRIS and TGCC in Paris and CINES in Montpellier was provided by GENCI (projects 609 and AD010813359). The authors ac-

knowledge the PSMN mesocenter in Lyon for CPU time and assistance (CPER/SYSPROD 2015-2022 project No. 2019-AURA-P5B and AXELERA Pôle de compétitivité).

## Supporting Information Available

Details on the calculation of the chemical potential of O<sub>2</sub>. Structures and details of the ceria-supported Pt<sub>x</sub>O<sub>y</sub> systems generated (Figure S1, S2, S4, and S5, Tables S1–S6). Structure of the gas-phase Pt<sub>13</sub> and Pt<sub>147</sub> clusters used as a starting point for the generation of ceria-supported Pt<sub>13</sub>O<sub>y</sub> and Pt<sub>147</sub>O<sub>y</sub> species (Figure S3). Bond analysis (Table S7).

## References

- (1) Vora, B. V. Development of Dehydrogenation Catalysts and Processes. Topics in Catalysis **2012**, *55*, 1297–1308.
- (2) Vilé, G.; Albani, D.; Almora-Barrios, N.; López, N.; Pérez-Ramírez, J. Advances in the Design of Nanostructured Catalysts for Selective Hydrogenation. ChemCatChem **2016**, *8*, 21–33.
- (3) Aranifard, S.; Ammal, S. C.; Heyden, A. On the importance of metal–oxide interface sites for the water–gas shift reaction over Pt/CeO<sub>2</sub> catalysts. Journal of Catalysis **2014**, *309*, 314–324.
- (4) Palma, V.; Ruocco, C.; Cortese, M.; Renda, S.; Meloni, E.; Festa, G.; Martino, M. Platinum Based Catalysts in the Water Gas Shift Reaction: Recent Advances. Metals **2020**, *10*, 866.
- (5) Xie, P.; Pu, T.; Nie, A.; Hwang, S.; Purdy, S. C.; Yu, W.; Su, D.; Miller, J. T.; Wang, C. Nanoceria-Supported Single-Atom Platinum Catalysts for Direct Methane Conversion. ACS Catalysis **2018**, *8*, 4044–4048.



- (6) Zhang, H.; Muravev, V.; Liu, L.; Liutkova, A.; Simons, J. F. M.; Detlefs, B.; Yang, H.; Kosinov, N.; Hensen, E. J. M. Pt/CeO<sub>2</sub> as Catalyst for Nonoxidative Coupling of Methane: Oxidative Regeneration. The Journal of Physical Chemistry Letters **2023**, 6778–6783.
- (7) Doumani, T. Dealkylation of Organic Compounds. Benzene from Toluene. Industrial & Engineering Chemistry **1958**, 50, 1677–1680.
- (8) Grenoble, D. C. The chemistry and catalysis of the toluene hydrodealkylation reaction I. The specific activities and selectivities of Group VIIB and Group VIII metals supported on alumina. Journal of Catalysis **1979**, 56, 32–39.
- (9) Barron, Y.; Maire, G.; Muller, J.; Gault, F. The mechanisms of hydrogenolysis and isomerization of hydrocarbons on metals II. Mechanisms of isomerization of hexanes on platinum catalysts. Journal of Catalysis **1966**, 5, 428–445.
- (10) Dautzenberg, F. M.; Platteeuw, J. Isomerization and dehydrocyclization of hexanes over monofunctional supported platinum catalysts. Journal of Catalysis **1970**, 19, 41–48.
- (11) Boubnov, A.; Dahl, S.; Johnson, E.; Molina, A. P.; Simonsen, S. B.; Cano, F. M.; Helveg, S.; Lemus-Yegres, L. J.; Grunwaldt, J.-D. Structure–activity relationships of Pt/Al<sub>2</sub>O<sub>3</sub> catalysts for CO and NO oxidation at diesel exhaust conditions. Applied Catalysis B: Environmental **2012**, 126, 315–325.
- (12) Liu, M.; Zhao, Z.; Duan, X.; Huang, Y. Nanoscale Structure Design for High-Performance Pt-Based ORR Catalysts. Advanced Materials **2019**, 31, 1802234.
- (13) Bartholomew, C. H. Mechanisms of catalyst deactivation. Applied Catalysis A: General **2001**, 212, 17–60.
- (14) Nagai, Y.; Hirabayashi, T.; Dohmae, K.; Takagi, N.; Minami, T.; Shinjoh, H.; Mat-

- sumoto, S. Sintering inhibition mechanism of platinum supported on ceria-based oxide and Pt-oxide-support interaction. Journal of Catalysis **2006**, 242, 103–109.
- (15) Dai, Y.; Lu, P.; Cao, Z.; Campbell, C. T.; Xia, Y. The physical chemistry and materials science behind sinter-resistant catalysts. Chemical Society Reviews **2018**, 47, 4314–4331.
- (16) Flynn, P. C.; Wanke, S. E. Experimental studies of sintering of supported platinum catalysts. Journal of Catalysis **1975**, 37, 432–448.
- (17) Straguzzi, G.; Aduriz, H.; Gigola, C. Redispersion of platinum on alumina support. Journal of Catalysis **1980**, 66, 171–183.
- (18) Arnal, P. M.; Comotti, M.; Schüth, F. High-Temperature-Stable Catalysts by Hollow Sphere Encapsulation. Angewandte Chemie International Edition **2006**, 45, 8224–8227.
- (19) Laursen, A. B.; Højholt, K. T.; Lundegaard, L. F.; Simonsen, S. B.; Helveg, S.; Schüth, F.; Paul, M.; Grunwaldt, J.-D.; Kegnaes, S.; Christensen, C. H.; Egeblad, K. Substrate Size-Selective Catalysis with Zeolite-Encapsulated Gold Nanoparticles. Angewandte Chemie **2010**, 122, 3582–3585.
- (20) Tong, L.; Chen, Z.-Q.; Zeng, W.-J.; Li, S.; Yang, Q.-Q.; Zhang, L.; Zhuang, X.; Chu, S.-Q.; Liang, H.-W. Microporous Sulfur-Doped Carbon Atoms as Supports for Sintering-Resistant Platinum Nanocluster Catalysts. ACS Applied Nano Materials **2021**, 4, 9489–9496.
- (21) Kalz, K. F.; Kraehnert, R.; Dvoyashkin, M.; Dittmeyer, R.; Gläser, R.; Krewer, U.; Reuter, K.; Grunwaldt, J.-D. Future Challenges in Heterogeneous Catalysis: Understanding Catalysts under Dynamic Reaction Conditions. ChemCatChem **2017**, 9, 17–29.

- (22) Hatanaka, M.; Takahashi, N.; Takahashi, N.; Tanabe, T.; Nagai, Y.; Suda, A.; Shinjoh, H. Reversible changes in the Pt oxidation state and nanostructure on a ceria-based supported Pt. Journal of Catalysis **2009**, 266, 182–190.
- (23) Cargnello, M.; Doan-Nguyen, V. V. T.; Gordon, T. R.; Diaz, R. E.; Stach, E. A.; Gorte, R. J.; Fornasiero, P.; Murray, C. B. Control of Metal Nanocrystal Size Reveals Metal-Support Interface Role for Ceria Catalysts. Science **2013**, 341, 771–773.
- (24) Nagai, Y.; Dohmae, K.; Ikeda, Y.; Takagi, N.; Tanabe, T.; Hara, N.; Guilera, G.; Pascarelli, S.; Newton, M. A.; Kuno, O.; Jiang, H.; Shinjoh, H.; Matsumoto, S. In Situ Redispersed of Platinum Autoexhaust Catalysts: An On-Line Approach to Increasing Catalyst Lifetimes? Angewandte Chemie International Edition **2008**, 47, 9303–9306.
- (25) Bruix, A. et al. Maximum Noble-Metal Efficiency in Catalytic Materials: Atomically Dispersed Surface Platinum. Angewandte Chemie International Edition **2014**, 53, 10525–10530.
- (26) Gänzler, A. M.; Casapu, M.; Vernoux, P.; Loridant, S.; Aires, F. J. C. S.; Epicier, T.; Betz, B.; Hoyer, R.; Grunwaldt, J.-D. Tuning the Structure of Platinum Particles on Ceria In Situ for Enhancing the Catalytic Performance of Exhaust Gas Catalysts. Angewandte Chemie International Edition **2017**, 56, 13078–13082.
- (27) Maurer, F.; Jelic, J.; Wang, J.; Gänzler, A.; Dolcet, P.; Wöll, C.; Wang, Y.; Studt, F.; Casapu, M.; Grunwaldt, J.-D. Tracking the formation, fate and consequence for catalytic activity of Pt single sites on CeO<sub>2</sub>. Nature Catalysis **2020**, 3, 824–833.
- (28) Hansen, T. W.; DeLaRiva, A. T.; Challa, S. R.; Datye, A. K. Sintering of Catalytic Nanoparticles: Particle Migration or Ostwald Ripening? Accounts of Chemical Research **2013**, 46, 1720–1730.
- (29) Johns, T. R.; Goeke, R. S.; Ashbacher, V.; Thüne, P. C.; Niemantsverdriet, J.; Kiefer, B.; Kim, C. H.; Balogh, M. P.; Datye, A. K. Relating adatom emission to

- improved durability of Pt–Pd diesel oxidation catalysts. Journal of Catalysis **2015**, 328, 151–164.
- (30) Jones, J.; Xiong, H.; DeLaRiva, A. T.; Peterson, E. J.; Pham, H.; Challa, S. R.; Qi, G.; Oh, S.; Wiebenga, M. H.; Hernández, X. I. P.; Wang, Y.; Datye, A. K. Thermally stable single-atom platinum-on-ceria catalysts via atom trapping. Science **2016**, 353, 150–154.
- (31) Behafarid, F.; Pandey, S.; Diaz, R. E.; Stach, E. A.; Cuenya, B. R. An in situ transmission electron microscopy study of sintering and redispersion phenomena over size-selected metal nanoparticles: environmental effects. Phys. Chem. Chem. Phys. **2014**, 16, 18176–18184.
- (32) Resasco, J.; DeRita, L.; Dai, S.; Chada, J. P.; Xu, M.; Yan, X.; Finzel, J.; Hanukovich, S.; Hoffman, A. S.; Graham, G. W.; Bare, S. R.; Pan, X.; Christopher, P. Uniformity Is Key in Defining Structure–Function Relationships for Atomically Dispersed Metal Catalysts: The Case of Pt/CeO<sub>2</sub>. Journal of the American Chemical Society **2020**, 142, 169–184.
- (33) Nie, L.; Mei, D.; Xiong, H.; Peng, B.; Ren, Z.; Hernandez, X. I. P.; DeLaRiva, A.; Wang, M.; Engelhard, M. H.; Kovarik, L.; Datye, A. K.; Wang, Y. Activation of surface lattice oxygen in single-atom Pt/CeO<sub>2</sub> for low-temperature CO oxidation. Science **2017**, 358, 1419–1423.
- (34) Qin, Y.; Su, Y. A DFT Study on Heterogeneous Pt/CeO<sub>2</sub>(110) Single Atom Catalysts for CO Oxidation. ChemCatChem **2021**, 13, 3857–3863.
- (35) Lu, Y.; Zhou, S.; Kuo, C.-T.; Kunwar, D.; Thompson, C.; Hoffman, A. S.; Boubnov, A.; Lin, S.; Datye, A. K.; Guo, H.; Karim, A. M. Unraveling the Intermediate Reaction Complexes and Critical Role of Support-Derived Oxygen Atoms in CO Oxidation on Single-Atom Pt/CeO<sub>2</sub>. ACS Catalysis **2021**, 11, 8701–8715.

- (36) Zhang, Z.; Tian, J.; Lu, Y.; Yang, S.; Jiang, D.; Huang, W.; Li, Y.; Hong, J.; Hoffman, A. S.; Bare, S. R.; Engelhard, M. H.; Datye, A. K.; Wang, Y. Memory-dictated dynamics of single-atom Pt on CeO<sub>2</sub> for CO oxidation. Nature Communications **2023**, 14, 2664.
- (37) Bruix, A.; Neyman, K. M.; Illas, F. Adsorption, Oxidation State, and Diffusion of Pt Atoms on the CeO<sub>2</sub>(111) Surface. The Journal of Physical Chemistry C **2010**, 114, 14202–14207.
- (38) Dvořák, F.; Camellone, M. F.; Tovt, A.; Tran, N.-D.; Negreiros, F. R.; Vorokhta, M.; Skála, T.; Matolínová, I.; Mysliveček, J.; Matolín, V.; Fabris, S. Creating single-atom Pt-ceria catalysts by surface step decoration. Nature Communications **2016**, 7, 10801.
- (39) Tovt, A.; Bagolini, L.; Dvořák, F.; Tran, N.-D.; Vorokhta, M.; Beranová, K.; Johánek, V.; Camellone, M. F.; Skála, T.; Matolínová, I.; Mysliveček, J.; Fabris, S.; Matolín, V. Ultimate dispersion of metallic and ionic platinum on ceria. Journal of Materials Chemistry A **2019**, 7, 13019–13028.
- (40) Wang, X.; van Bokhoven, J. A.; Palagin, D. Atomically dispersed platinum on low index and stepped ceria surfaces: phase diagrams and stability analysis. Physical Chemistry Chemical Physics **2020**, 22, 28–38.
- (41) Toyoda, E.; Jinnouchi, R.; Hatanaka, T.; Morimoto, Y.; Mitsuhara, K.; Visikovskiy, A.; Kido, Y. The d-Band Structure of Pt Nanoclusters Correlated with the Catalytic Activity for an Oxygen Reduction Reaction. The Journal of Physical Chemistry C **2011**, 115, 21236–21240.
- (42) Li, L.; Larsen, A. H.; Romero, N. A.; Morozov, V. A.; Glinsvad, C.; Abild-Pedersen, F.; Greeley, J.; Jacobsen, K. W.; Nørskov, J. K. Investigation of Catalytic Finite-Size-Effects of Platinum Metal Clusters. The Journal of Physical Chemistry Letters **2013**, 4, 222–226.

- (43) Calle-Vallejo, F.; Martínez, J. I.; García-Lastra, J. M.; Sautet, P.; Loffreda, D. Fast Prediction of Adsorption Properties for Platinum Nanocatalysts with Generalized Coordination Numbers. Angewandte Chemie International Edition **2014**, 53, 8316–8319.
- (44) Lentz, C.; Jand, S. P.; Melke, J.; Roth, C.; Kaghazchi, P. DRIFTS study of CO adsorption on Pt nanoparticles supported by DFT calculations. Journal of Molecular Catalysis A: Chemical **2017**, 426, 1–9.
- (45) Verga, L. G.; Aarons, J.; Sarwar, M.; Thompsett, D.; Russell, A. E.; Skylaris, C.-K. DFT calculation of oxygen adsorption on platinum nanoparticles: coverage and size effects. Faraday Discussions **2018**, 208, 497–522.
- (46) Bruix, A.; Rodriguez, J. A.; Ramírez, P. J.; Senanayake, S. D.; Evans, J.; Park, J. B.; Stacchiola, D.; Liu, P.; Hrbek, J.; Illas, F. A New Type of Strong Metal–Support Interaction and the Production of H<sub>2</sub> through the Transformation of Water on Pt/CeO<sub>2</sub> (111) and Pt/CeO<sub>x</sub>/TiO<sub>2</sub>(110) Catalysts. Journal of the American Chemical Society **2012**, 134, 8968–8974.
- (47) Kunwar, D. et al. Stabilizing High Metal Loadings of Thermally Stable Platinum Single Atoms on an Industrial Catalyst Support. ACS Catalysis **2019**, 9, 3978–3990.
- (48) Yoon, S.; Ha, H.; Kim, J.; Nam, E.; Yoo, M.; Jeong, B.; Kim, H. Y.; An, K. Influence of the Pt size and CeO<sub>2</sub> morphology at the Pt–CeO<sub>2</sub> interface in CO oxidation. Journal of Materials Chemistry A **2021**, 9, 26381–26390.
- (49) Castro-Latorre, P.; Neyman, K. M.; Bruix, A. Systematic Characterization of Electronic Metal–Support Interactions in Ceria-Supported Pt Particles. The Journal of Physical Chemistry C **2023**, 127, 17700–17710.
- (50) Zandkarimi, B.; Poths, P.; Alexandrova, A. N. When Fluxionality Beats Size Selection: Acceleration of Ostwald Ripening of Sub-Nano Clusters. Angewandte Chemie International Edition **2021**, 60, 11973–11982.

- (51) Kozlov, S. M.; Aleksandrov, H. A.; Goniakowski, J.; Neyman, K. M. Effect of MgO(100) support on structure and properties of Pd and Pt nanoparticles with 49–155 atoms. The Journal of Chemical Physics **2013**, 139, 084701.
- (52) Neyman, K. M.; Kozlov, S. M. Quantifying interactions on interfaces between metal particles and oxide supports in catalytic nanomaterials. NPG Asia Materials **2022**, 14, 59.
- (53) Bosio, N.; Di, M.; Skoglundh, M.; Carlsson, P.-A.; Grönbeck, H. Interface Reactions Dominate Low-Temperature CO Oxidation Activity over Pt/CeO<sub>2</sub>. The Journal of Physical Chemistry C **2022**, 126, 16164–16171.
- (54) Kresse, G.; Hafner, J. Ab initio molecular dynamics for liquid metals. Physical Review B **1993**, 47, 558–561.
- (55) Kresse, G.; Furthmüller, J. Efficient iterative schemes for ab initio total-energy calculations using a plane-wave basis set. Physical Review B **1996**, 54, 11169–11186.
- (56) Perdew, J. P.; Ernzerhof, M.; Burke, K. Rationale for mixing exact exchange with density functional approximations. The Journal of Chemical Physics **1996**, 105, 9982–9985.
- (57) Grimme, S.; Antony, J.; Ehrlich, S.; Krieg, H. A consistent and accurate ab initio parametrization of density functional dispersion correction (DFT-D) for the 94 elements H-Pu. The Journal of Chemical Physics **2010**, 132, 154104.
- (58) Effect of the damping function in dispersion corrected density functional theory. Journal of Computational Chemistry **2011**, 32, 1456–1465.
- (59) Kresse, G.; Joubert, D. From ultrasoft pseudopotentials to the projector augmented-wave method. Physical Review B **1999**, 59, 1758–1775.

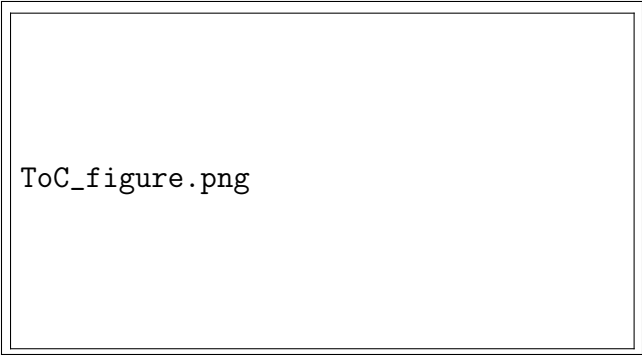
- (60) Dudarev, S. L.; Botton, G. A.; Savrasov, S. Y.; Humphreys, C. J.; Sutton, A. P. Electron-energy-loss spectra and the structural stability of nickel oxide: An LSDA+U study. Physical Review B **1998**, 57, 1505–1509.
- (61) Skorodumova, N. V.; Simak, S. I.; Lundqvist, B. I.; Abrikosov, I. A.; Johansson, B. Quantum Origin of the Oxygen Storage Capability of Ceria. Physical Review Letters **2002**, 89, 166601.
- (62) Nolan, M.; Parker, S. C.; Watson, G. W. The electronic structure of oxygen vacancy defects at the low index surfaces of ceria. Surface Science **2005**, 595, 223–232, Explicación de por qué es necesario el parámetro de Hubbard.
- (63) Loschen, C.; Carrasco, J.; Neyman, K. M.; Illas, F. First-principles LDA+U and GGA+U study of cerium oxides: Dependence on the effective U parameter. Physical Review B - Condensed Matter and Materials Physics **2007**, 75, 1–8.
- (64) Ganduglia-Pirovano, M. V.; Hofmann, A.; Sauer, J. Oxygen vacancies in transition metal and rare earth oxides: Current state of understanding and remaining challenges. Surface Science Reports **2007**, 62, 219–270.
- (65) Ganduglia-Pirovano, M. V.; Silva, J. L. F. D.; Sauer, J. Density-Functional Calculations of the Structure of Near-Surface Oxygen Vacancies and Electron Localization on CeO<sub>2</sub>(111). Physical Review Letters **2009**, 102, 026101.
- (66) Fabris, S.; Vicario, G.; Balducci, G.; de Gironcoli, S.; Baroni, S. Electronic and Atomistic Structures of Clean and Reduced Ceria Surfaces. The Journal of Physical Chemistry B **2005**, 109, 22860–22867.
- (67) Cococcioni, M.; de Gironcoli, S. Linear response approach to the calculation of the effective interaction parameters in the LDA+U method. Physical Review B **2005**, 71, 035105.



- (68) Feng, Y.; Wan, Q.; Xiong, H.; Zhou, S.; Chen, X.; Hernandez, X. I. P.; Wang, Y.; Lin, S.; Datye, A. K.; Guo, H. Correlating DFT Calculations with CO Oxidation Reactivity on Ga-Doped Pt/CeO<sub>2</sub> Single-Atom Catalysts. The Journal of Physical Chemistry C **2018**, 122, 22460–22468.
- (69) Gänzler, A. M.; Casapu, M.; Maurer, F.; Störmer, H.; Gerthsen, D.; Ferré, G.; Vernoux, P.; Bornmann, B.; Frahm, R.; Murzin, V.; Nachtegaal, M.; Votsmeier, M.; Grunwaldt, J.-D. Tuning the Pt/CeO<sub>2</sub> Interface by in Situ Variation of the Pt Particle Size. ACS Catalysis **2018**, 8, 4800–4811.
- (70) Zhang, Z.; Wei, Z.; Sautet, P.; Alexandrova, A. N. Hydrogen-Induced Restructuring of a Cu(100) Electrode in Electroreduction Conditions. Journal of the American Chemical Society **2022**, 144, 19284–19293.
- (71) Cardona, J. E. M.; Salichon, A.; Tarrat, N.; Gaudry, E.; Loffreda, D. Structural, Ordering, and Magnetic Properties of PtNi Nanoalloys Explored by Density Functional Theory and Stability Descriptors. The Journal of Physical Chemistry C **2023**, 127, 18043–18057.
- (72) Reuter, K.; Scheffler, M. Composition and structure of the RuO<sub>2</sub>(110) surface in an surface in an O<sub>2</sub> and CO environment: Implications for the catalytic formation of CO<sub>2</sub>. Physical Review B **2003**, 68, 045407.
- (73) Hellier, A.; Chizallet, C.; Raybaud, P. PtO<sub>x</sub>Cl<sub>y</sub>(OH)<sub>z</sub>(H<sub>2</sub>O)<sub>n</sub> Complexes under Oxidative and Reductive Conditions: Impact of the Level of Theory on Thermodynamic Stabilities. ChemPhysChem **2023**, 24.
- (74) Goldsmith, B. R.; Sanderson, E. D.; Ouyang, R.; Li, W.-X. CO- and NO-Induced Disintegration and Redispersion of Three-Way Catalysts Rhodium, Palladium, and Platinum: An ab Initio Thermodynamics Study. The Journal of Physical Chemistry C **2014**, 118, 9588–9597.

- (75) Zhou, X.; Zhang, Y.; Wang, J. DFT study on the regeneration of Pt/ $\gamma$ -Al<sub>2</sub>O<sub>3</sub> catalyst: The effect of chlorine on the redispersion of metal species. Applied Surface Science **2021**, 545, 148988.
- (76) Daelman, N.; Capdevila-Cortada, M.; López, N. Dynamic charge and oxidation state of Pt/CeO<sub>2</sub> single-atom catalysts. Nature Materials **2019**, 18, 1215–1221.
- (77) Reddy, K. P.; Choi, H.; Kim, D.; Choi, M.; Ryoo, R.; Park, J. Y. The facet effect of ceria nanoparticles on platinum dispersion and catalytic activity of methanol partial oxidation. Chemical Communications **2021**, 57, 7382–7385.

## TOC Graphic



ToC\_figure.png

# TOC Graphic

